Robust flow measurement with multi-exposure speckle imaging

Ashwin B. Parthasarathy, W. James Tom, Ashwini Gopal, Xiaojing Zhang and Andrew K. Dunn

Department of Biomedical Engineering, The University of Texas at Austin
Austin, TX, 78712
adunn@mail.utexas.edu

Abstract: Laser Speckle Contrast Imaging (LSCI) is a minimally invasive full field optical technique used to generate blood flow maps with high spatial and temporal resolution. The lack of quantitative accuracy and the inability to predict flows in the presence of static scatterers such as an intact or thinned skull have been the primary limitation of LSCI. We present a new Multi-Exposure Speckle Imaging (MESI) instrument that has potential to obtain quantitative baseline flow measures. We show that the MESI instrument extends the range over which relative flow measurements are linear. We also present a new speckle model which can discriminate flows in the presence of static scatters. We show that in the presence of static scatterers the new model used along with the new MESI instrument can predict correlation times of flow consistently to within 10% of the value without static scatterers compared to an average deviation of more than 100% from the value without static scatterers using traditional LSCI. We also show that the new speckle model used with the MESI instrument can maintain the linearity of relative flow measurements in the presence of static scatterers.

© 2008 Optical Society of America

OCIS codes: (030.6140)Speckle; (110.6150)Speckle imaging; (120.6160)Speckle interferometry; (120.5820)Scattering measurements; (170.6480)Spectroscopy, speckle; (170.3890)Medical optics instrumentation; (999.9999)Flow Measurements

---

References and links

1. A. Fercher and J. Briers, "Flow visualization by means of single-exposure speckle photography," Opt. Commun. **37**, 326–330 (1981).
2. A. Dunn, H. Bolay, M. Moskowitz, and D. Boas, "Dynamic Imaging of Cerebral Blood Flow Using Laser Speckle," J. Cereb. Blood Flow Metab. **21**, 195–201 (2001).
3. B. Weber, C. Burger, M. Wyss, G. von Schulthess, F. Scheffold, and A. Buck, "Optical imaging of the spatiotemporal dynamics of cerebral blood flow and oxidative metabolism in the rat barrel cortex," Eur. J. Neurosci. **20**, 2664–2670 (2004).
4. T. Durduran, M. Burnett, G. Yu, C. Zhou, D. Furuya, A. Yodh, J. Detre, and J. Greenberg, "Spatiotemporal Quantification of Cerebral Blood Flow During Functional Activation in Rat Somatosensory Cortex Using Laser-Speckle Flowmetry," J. Cereb. Blood Flow Metab. **24**, 518–525 (2004).
5. D. Atochin, J. Murciano, Y. Gursoy-Ozdemir, T. Krasik, F. Noda, C. Ayata, A. Dunn, M. Moskowitz, P. Huang, and V. Muzykantov, "Mouse Model of Microembolic Stroke and Reperfusion," Stroke **35**, 2177–2182 (2004).
6. A. Kharlamov, B. Brown, K. Easley, and S. Jones, "Heterogeneous response of cerebral blood flow to hypotension demonstrated by laser speckle imaging flowmetry in rats," Neurosci. Lett **368**, 151–156 (2004).
7. K. Murari, N. Li, A. Rege, X. Jia, A. All, and N. Thakor, "Contrast-enhanced imaging of cerebral vasculature with laser speckle," Appl. Opt. **46**, 5340–5346 (2007).

8. B. Ruth, "Measuring the steady-state value and the dynamics of the skin blood flow using the non-contact laser speckle method." Med. Eng. Phys. **16**, 105–11 (1994).

9. K. Forrester, C. Stewart, J. Tulip, C. Leonard, and R. Bray, "Comparison of laser speckle and laser Doppler perfusion imaging: Measurement in human skin and rabbit articular tissue," Med. Biol. Engg. Comp. **40**, 687–697 (2002).

10. B. Choi, N. Kang, and J. Nelson, "Laser speckle imaging for monitoring blood flow dynamics in the in vivo rodent dorsal skin fold model," Microvasc. Res **68**, 143–146 (2004).

11. K. Yaoeda, M. Shirakashi, S. Funaki, H. Funaki, T. Nakatsue, A. Fukushima, and H. Abe, "Measurement of microcirculation in optic nerve head by laser speckle flowgraphy in normal volunteers," Am. J. Opthalmol. **130**, 606–610 (2000).

12. C. Ayata, A. Dunn, Y. Gursoy-Ozdemir, Z. Huang, D. Boas, and M. Moskowitz, "Laser speckle flowmetry for the study of cerebrovascular physiology in normal and ischemic mouse cortex," J. Cereb. Blood Flow Metab. **24**, 744–755 (2004).

13. A. Strong, E. Bezzina, P. Anderson, M. Boutelle, S. Hopwood, and A. Dunn, "Evaluation of laser speckle flowmetry for imaging cortical perfusion in experimental stroke studies: quantitation of perfusion and detection of peri-infarct depolarisations," J. Cereb. Blood Flow Metab. **26**, 645–53 (2006).

14. A. Dunn, A. Devor, A. Dale, and D. Boas, "Spatial extent of oxygen metabolism and hemodynamic changes during functional activation of the rat somatosensory cortex," NeuroImage **27**, 279–290 (2005).

15. S. Yuan, A. Devor, D. Boas, and A. Dunn, "Determination of optimal exposure time for imaging of blood flow changes with laser speckle contrast imaging," Appl. Opt. **44**, 1823–1830 (2005).

16. M. Stern, "In vivo evaluation of microcirculation by coherent light scattering," Nature (London) **254**, 56–8 (1975).

17. H. Shin, P. Jones, M. Garcia-Alloza, L. Borrelli, S. Greenberg, B. Bacskai, M. Frosch, B. Hyman, M. Moskowitz, and C. Ayata, "Age-dependent cerebrovascular dysfunction in a transgenic mouse model of cerebral amyloid angiopathy," Brain **130**, 2310–2319 (2007).

18. R. Bandyopadhyay, A. Gittings, S. Suh, P. Dixon, and D. Durian, "Speckle-visibility spectroscopy: A tool to study time-varying dynamics," Rev. Sci. Instrum. **76**, 093110 (2005).

19. B. Berne and R. Pecora, *Dynamic Light Scattering : with Applications to Chemistry, Biology and Physics* (Dover Publications, 2000).

20. R. Bonner and R. Nossal, "Model for laser Doppler measurements of blood flow in tissue," Appl. Opt. **20**, 2097–2107 (1981).

21. K. Forrester, J. Tulip, C. Leonard, C. Stewart, and R. Bray, "A laser speckle imaging technique for measuring tissue perfusion," IEEE Trans. Biomed. Engg. **51**, 2074–2084 (2004).

22. P. Dixon and D. Durian, "Speckle Visibility Spectroscopy and Variable Granular Fluidization," Phys. Rev. Lett. **90**, 184302 (2003).

23. P. Lemieux and D. Durian, "Investigating non-Gaussian scattering processes by using n th-order intensity correlation functions," J. Opt. Soc. Am. A **16**, 1651–1664 (1999).

24. H. Cheng, Q. Luo, S. Zeng, S. Chen, J. Cen, and H. Gong, "Modified laser speckle imaging method with improved spatial resolution," J. Biomed. Opt. **8**, 559–564 (2003).

25. P. Li, S. Ni, L. Zhang, S. Zeng, and Q. Luo, "Imaging cerebral blood flow through the intact rat skull with temporal laser speckle imaging," Opt. Lett. **31**, 1824–1826 (2006).

26. P. Zakharov, A. Völker, A. Buck, B. Weber, and F. Scheffold, "Quantitative modeling of laser speckle imaging," Opt. Lett. **31**, 3465–3467 (2006).

27. D. Boas and A. Yodh, "Spatially varying dynamical properties of turbid media probed with diffusing temporal light correlation," J. Opt. Soc. Am. A **14**, 192–215 (1997).

28. J. Anderson, D. Chiu, R. Jackman, O. Cherniavskaya, J. McDonald, H. Wu, S. Whitesides, and G. Whitesides, "Fabrication of Topologically Complex Three-Dimensional Microfluidic Systems in PDMS by Rapid Prototyping," Science **261**, 895 (1993).

29. A. Oldenburg, F. Toublan, K. Suslick, A. Wei, and S. Boppart, "Magnetomotive contrast for in vivo optical coherence tomography," Opt. Express **13**, 6597–6614 (2005).

1. Introduction

Laser Speckle Contrast Imaging (LSCI) is a popular optical technique to image blood flow. It was introduced by Fercher and Briers [1] in 1981, and has since been used to image blood flow in the brain [2–7], skin [8–10] and retina [11]. Since LSCI is a full field imaging technique, its spatial resolution is not at the expense of scanning time unlike more traditional flow measurement techniques like scanning Laser Doppler Imaging (LDI). For these reasons LSCI has been used to quantify the cerebral blood flow (CBF) changes in stroke models in the rat [2] and mouse brain [12, 13] and for functional activation studies [4, 14, 15].

Laser speckle is a random interference pattern produced by the coherent addition of scattered laser light with slightly different path lengths. Motion of these scattering particles cause spatial and temporal modifications of the speckle pattern, either of which can be used to detect the speed of the scatterers [1, 16]. In the spatial domain, these modifications manifest themselves as localized blurring of the image. LSCI quantifies the extent of this localized spatial blurring by calculating a quantity called speckle contrast (K) over a small window (usually 7×7 pixels) of the image.

$$K = \frac{\sigma_s}{\langle I \rangle}, \tag{1}$$

where σ_s is the standard deviation and $\langle I \rangle$ is the mean of the pixels of the window. For slower speeds, the pixels decorrelate less and hence K is large and vice versa.

One limitation or criticism of LSCI is that it can produce good measures of relative flow but cannot measure baseline flows. This has prevented comparisons of LSCI measurements to be carried out across animals or species and across different studies [17]. Lack of baseline measures also make calibration difficult [13]. This limitation has been attributed to the use of an approximate model for measurements [18]. Another limitation of LSCI, especially for imaging cerebral blood flow, has been the inability of traditional speckle models to predict accurate flows in the presence of light scattered from static tissue elements. Traditionally this problem has been avoided in imaging cerebral blood flow by performing a full craniotomy (removal of skull) on the animal. Such a procedure is traumatic for the animal and can disturb normal physiological conditions. Imaging through an intact yet thinned skull can drastically improve experimental conditions by (a) being less traumatic to the animal, (b) reducing the impact of surgery on normal physiological conditions and (c) enable chronic and long term studies [17]. One of the advantages of imaging CBF in mice is that LSCI can be performed through an intact skull [12]. However variations in skull thickness lead to significant variability in speckle contrast values.

We present a new speckle imaging instrument and a new speckle expression that could help overcome these limitations. The influence of speed of the particles on speckle contrast can be quantitatively described using the theory of dynamic light scattering (DLS) [19] through correlation times (τ_c). The correlation time of speckles is the characteristic decay time of the speckle autocorrelation function. The speckle correlation function is a function that describes the dynamics of the system using backscattered coherent light. Under conditions of single scattering from moving particles, small scattering angles and strong tissue scattering, the correlation time can be shown to be inversely proportional to the mean translational velocity of the scatterers [20]. Strictly speaking this assumption that $\tau_c \propto \frac{1}{v}$ (where v is the mean velocity) is most appropriate for capillaries where a photon is more likely to scatter off only one moving particle and succeeding phase shifts of photons are totally independent of earlier ones [20]. Hence great care should be observed when using this expression. We believe that our measurements are made in channels that mimic smaller blood vessels, hence this relation between the correlation time and velocity can indeed be used.

The uncertainty over the relation between correlation time and velocity is a fundamental limitation for all DLS based flow measurement techniques. Nevertheless, quantitative flow measurements can be performed through accurate estimation of correlation times. The correlation times can be related to velocities through external calibration. The speckle contrast can be expressed in terms of the correlation time of speckles and the exposure duration of the camera [1, 18]. Our new instrument obtains speckle images at different exposure durations and uses this multi-exposure data to quantify τ_c. Previous efforts to obtain speckle images at multiple exposure durations have been limited to a few durations [21] or to line scan cameras [18, 22]. We present a new technique to obtain images over a wide range of exposure durations (50 μs to

80 ms). To our knowledge this is the first instrument to obtain 2D speckle images over almost 3 decades of exposure durations. We use this *Multi-Exposure Speckle Imaging (MESI) instrument* to obtain better estimates of correlation times of speckles. Using this new instrument and a new speckle model, we show that we can increase the range over which relative correlation time measurements are linear.

We also develop a new speckle model that accounts for the presence of light scattered from static particles. Our new model applies the theory of time integrated speckle to previous work [23] on static scattered light. Cheng et. al. [24] and Li et. al. [25] showed increased visibility of blood vessels using LSCI when a temporal processing scheme was used. However, they did not quantify the extent to which their technique was accurate or consistent in predicting flows. Zakharov et. al. [26] showed that the influence of static scatterers can be accounted for by using a different speckle model, and cross correlating one speckle image with another which is significantly displaced in time. We note that our model is similar to the one developed by Zakharov et. al [26], but that our model introduces previously neglected contributions due to nonergodic light and experimental noise. We also identify that the assumption on ergodicity breaks down in the presence of static scatterers and propose a solution to account for nonergodic light. We provide a technique to model and account for experimental noise. The influence of noise and nonergodic light has been neglected in most previous studies. We perform a comprehensive study with a novel tissue phantom to show that the new model used in conjunction with the Multi-Exposure Speckle Imaging (MESI) instrument can predict correlation times consistently in the presence of static speckles.

2. A robust speckle model

In their introductory paper on speckle [1], Fercher and Briers related speckle contrast to the exposure duration of the camera and correlation time of the speckles, using the theory of correlation functions and time integrated speckle. The theory of correlation functions has been widely used in dynamic light scattering (DLS) [19] and LSCI is a direct extension of it. The temporal fluctuations of speckles can be quantified using the electric field autocorrelation function $g_1(\tau)$. Typically $g_1(\tau)$ is difficult to measure and the intensity autocorrelation function $g_2(\tau)$ is recorded. The field and intensity autocorrelation functions are related through the Siegert relation [19].

$$g_2(\tau) = 1 + \beta |g_1(\tau)|^2, \tag{2}$$

where β is a normalization factor which accounts for speckle averaging due to mismatch of speckle size and detector size, polarization and coherence effects. Fercher and Briers [1] assumed that $\beta = 1$, used Eq. 2 and the fact that the recorded intensity is integrated over the exposure duration to derive the first speckle model.

$$K(T, \tau_c) = \left(\frac{1 - e^{-2x}}{2x} \right)^{1/2}, \tag{3}$$

where $x = T/\tau_c$, T is the exposure duration of the camera and τ_c is the correlation time. Eq. 3 has been widely used to determine relative blood flow changes for LSCI measurements.

Recently, Bandyopadhyay et. al. [18] showed that this formulation (Eq. 3) did not account for speckle averaging effects. They argued that β should not be ignored and also used triangular weighting of the autocorrelation function to develop a more rigorous model relating speckle contrast to τ_c:

$$K(T, \tau_c) = \left(\beta \frac{e^{-2x} - 1 + 2x}{2x^2} \right)^{1/2}. \tag{4}$$

One disadvantage of these models is that they breakdown in the presence of statically scattered light. This is primarily because these models rely on the Siegert relation (Eq. 2) which assumes that the speckles follow Gaussian statistics in time. In the presence of static scatterers, the fluctuations of the scattered field remain Gaussian but the intensity acquires an extra static contribution causing the recorded intensity to deviate from Gaussian statistics, and hence the Siegert relation (Eq. 2) cannot be applied [23, 27]. This can be corrected by modeling the scattered field [23, 27] as

$$E_h(t) = E(t) + E_s e^{-i\omega_0 t}, \tag{5}$$

where $E(t)$ is the Gaussian fluctuation, E_s is the static field amplitude and ω_0 is the source frequency. The Siegert relation can now be modified as [23, 27]

$$
\begin{aligned}
g_2^h(\tau) &= 1 + \frac{\beta}{(I_f + I_s)^2} \left[I_f^2 |g_1(\tau)|^2 + 2I_f I_s |g_1(\tau)| \right] \\
&= 1 + A\beta |g_1(\tau)|^2 + B\beta |g_1(\tau)|, \tag{6}
\end{aligned}
$$

where $A = \dfrac{I_f^2}{(I_f + I_s)^2}$ and $B = \dfrac{2I_f I_s}{(I_f + I_s)^2}$, $I_s = E_s E_s^*$ represents contribution from the static scattered light, and $I_f = \langle EE^* \rangle$ represents contribution from the dynamically scattered light.

This updated Siegert relation can be used to derive the relation between speckle variance and correlation time as with the other models [18, 22]. Following the approach of Bandyopadhyay et. al. [18] the second moment of intensity can be written using the modified Siegert relation as

$$
\begin{aligned}
\langle I^2 \rangle_T &\equiv \left\langle \int_0^T \int_0^T I_i(t') I_i(t'') dt' dt'' / T^2 \right\rangle_i \\
&= \langle I \rangle^2 \int_0^T \int_0^T \left[1 + A\beta \left(g_1(t' - t'') \right)^2 + B\beta g_1(t' - t'') \right] dt' dt'' / T^2. \tag{7}
\end{aligned}
$$

The reduced second moment of intensity or the variance is hence

$$v_2(T) \equiv \int_0^T \int_0^T \left[A\beta \left(g_1(t' - t'') \right)^2 + B\beta g_1(t' - t'') \right] dt' dt'' / T^2. \tag{8}$$

Since $g_1(t)$ is an even function, the double integral simplifies to [22]

$$v_2(T) = A\beta \int_0^T 2 \left(1 - \frac{t}{T} \right) [g_1(t)]^2 \frac{dt}{T} + B\beta \int_0^T 2 \left(1 - \frac{t}{T} \right) [g_1(t)] \frac{dt}{T}. \tag{9}$$

We note that this expression (Eq. 9) represents a *new speckle visibility expression* that accounts for the varying proportions of light scattered from static and dynamic scatterers. Assuming that the velocities of the scatterers have a Lorentzian distribution [1], which gives $g_1(t) = e^{-t/\tau_c}$ and recognizing that the square root of the variance is the speckle contrast [18], Eq. 9 can be simplified to:

$$K(T, \tau_c) = \left\{ \beta \rho^2 \frac{e^{-2x} - 1 + 2x}{2x^2} + 4\beta \rho (1 - \rho) \frac{e^{-x} - 1 + x}{x^2} \right\}^{1/2}, \tag{10}$$

where $x = \frac{T}{\tau_c}$, $\rho = \frac{I_f}{(I_f + I_s)}$ is the fraction of total light that is dynamically scattered, β is a normalization factor to account for speckle averaging effects, T is the camera exposure duration and τ_c is the correlation time of the speckles.

When there are no static scatterers present, $\rho \to 1$ and Eq. 10 simplifies to Eq. 4. However Eq. 10 is incomplete since in the limit that only static scatterers are present ($\rho \to 0$), it does not reduce to a constant speckle contrast value as one would expect for spatial speckle contrast. This can be explained by recognizing that K in Eq. 10 refers to the temporal (temporally sampled) speckle contrast. Our initial definition of K (Eq. 1) was based on spatial sampling of speckles. Traditionally in LSCI, speckle contrast has been estimated through spatial sampling, by assuming ergodicity to replace temporal sampling of speckles with an ensemble sampling [1]. In the presence of static scatterers this assumption is no longer valid [27]. We would prefer to use spatial (ensemble sampled) speckle contrast since it helps retain the temporal resolution of LSCI. In order for our theory to be used with spatial (ensemble sampled) speckle contrast, we propose that a constant term be added to the speckle visibility expression (Eq. 9). We refer to this constant as *nonergodic variance* (v_{ne}). We assume that this is constant in time.

The speckle pattern obtained from a completely static sample does not fluctuate. Hence the variance of the speckle signal over time is zero as predicted by Eq. 10. However the spatial (or ensemble) speckle contrast would be a nonzero constant due to spatial averaging of the random interference pattern produced. This nonzero constant (v_{ne}) would primarily be determined by the sample, illumination and imaging geometries. Since the speckle contrast is normalized to the integrated intensity, v_{ne} would not depend on the integrated intensity. These factors are clearly independent of the exposure duration of the camera, and hence our assumption is quite valid. The addition of v_{ne} should enable us to continue using spatial (or ensemble) speckle contrast in the presence of static scatterers. Later in this paper we will demonstrate the validity of approximating the nonergodic contribution by a constant. We note that this addition of the nonergodic variance is a significant improvement over existing models.

An additional factor that has been neglected is experimental noise which can have a significant impact on measured speckle contrast. Experimental noise can be broadly categorized into shot noise and camera noise. Shot noise is the largest contributor of noise, and it is primarily determined by the signal level at the pixels. This can be held independent of exposure duration, by equalizing the intensity of the image across different exposure durations. Camera noise includes readout noise, QTH noise, Johnson noise etc. It can also be made independent of exposure by holding the camera exposure duration constant. In section 3 we present an instrument that holds camera exposure duration constant, yet obtains multi-exposure speckle images by pulsing the laser, while maintaining the same intensity over all exposure durations. Hence the experimental noise will add an additional constant spatial variance, v_{noise}.

In the light of these arguments, we can rewrite Eq. 10 as:

$$K(T, \tau_c) = \left\{ \beta \rho^2 \frac{e^{-2x} - 1 + 2x}{2x^2} + 4\beta \rho (1 - \rho) \frac{e^{-x} - 1 + x}{x^2} + v_{ne} + v_{noise} \right\}^{1/2}, \quad (11)$$

where $x = \frac{T}{\tau_c}$, $\rho = \frac{I_f}{(I_f + I_s)}$ is the fraction of total light that is dynamically scattered, β is a normalization factor to account for speckle averaging effects, T is the camera exposure duration, τ_c is the correlation time of the speckles, v_{noise} is the constant variance due to experimental noise and v_{ne} is the constant variance due to nonergodic light.

Eq. 11 is a rigorous and practical *robust speckle model* that accounts for the presence of static scattered light, experimental noise and nonergodic variance due to the ensemble averaging. We also recognize that while v_{ne} and v_{noise} make the model more complete, they do not add any new information about the dynamics of the system, all of which is held in τ_c. Hence we can view v_{ne} and v_{noise} as experimental variables/artifacts. In our ensuing discussions, we often lump them together as a single static spatial variance v_s, where $v_s = v_{ne} + v_{noise}$.
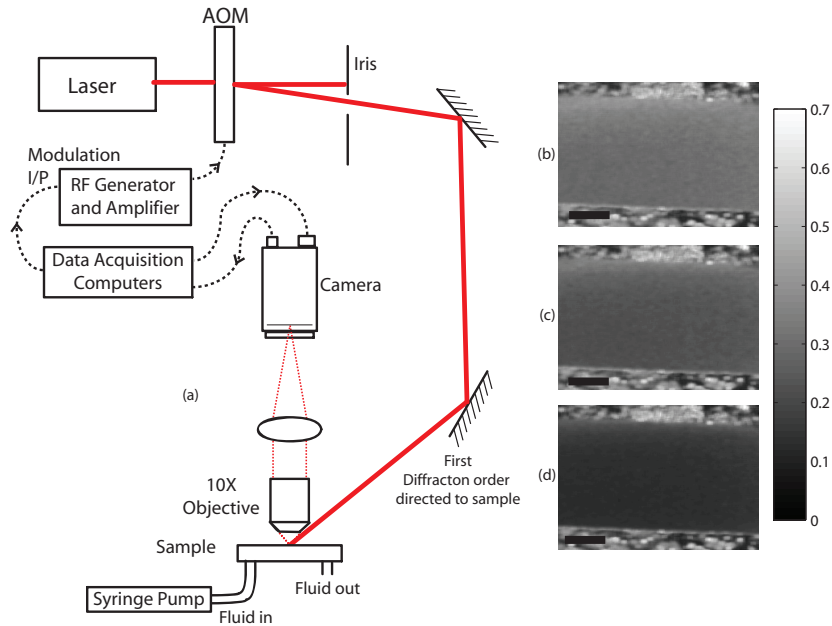
Fig. 1. Multi-Exposure Speckle Imaging instrument (a) Schematic (b) Speckle Contrast image at 0.1 ms exposure duration (c) Speckle Contrast image at 5 ms exposure duration (d) Speckle Contrast image at 40 ms exposure duration (scale bar = 50 μm)

3. Multi-exposure speckle imaging instrument

The objective for developing a new speckle imaging instrument is based on the need to acquire images that will obtain correlation time information. The requirements include varying the exposure duration, maintaining a constant intensity over a wide range of exposures and ensuring that the noise variance is constant. In order to test the model experimentally, we performed flow measurements on microfluidic flow phantoms. To do this, the exposure duration of speckle measurements had to be changed, while ensuring that our conditions were satisfied. To obtain speckle images at multiple exposure durations we fixed the actual camera exposure duration and gated a laser diode during each exposure to effectively vary the speckle exposure duration T as in Yuan et. al. [15]. This approach ensures that the camera noise variance and the average image intensity are constant. Directly pulsing the laser limited the range of exposure durations that can be achieved. The lasing threshold of the laser diode dictated the minimum intensity and hence the maximum exposure duration that can be recorded. Consequently, the minimum exposure duration would be limited by the dynamic range of the instruments. To overcome this limitation the laser was pulsed through an acousto optic modulator (AOM). By modulating the amplitude of the RF wave fed to the AOM, the intensity of the first diffraction order can be varied, enabling control over both the integrated intensity and the effective exposure duration.

Figure 1 provides a schematic of the experimental setup. A diode laser beam (Hitachi HL6535MG; λ=658nm, 80mW Thorlabs, Newton, NJ, USA) was directed to an acousto optic modulator (AOM) (IntraAction Corp., BellWood, IL, USA). The AOM was driven by signals generated from an RF AOM Modulator driver (IntraAction Corp., BellWood, IL, USA) and the first diffraction order was directed toward the sample. The sample was imaged using a 10X ∞ corrected objective (Thorlabs, Newton, NJ, USA) and a 150mm tube lens (Thorlabs, Newton, NJ, USA). Images were acquired using a camera (Basler 602f; Basler Vision Technologies,

Germany). Software was written to control the timing of the AOM pulsing and synchronize it with image acquisition.
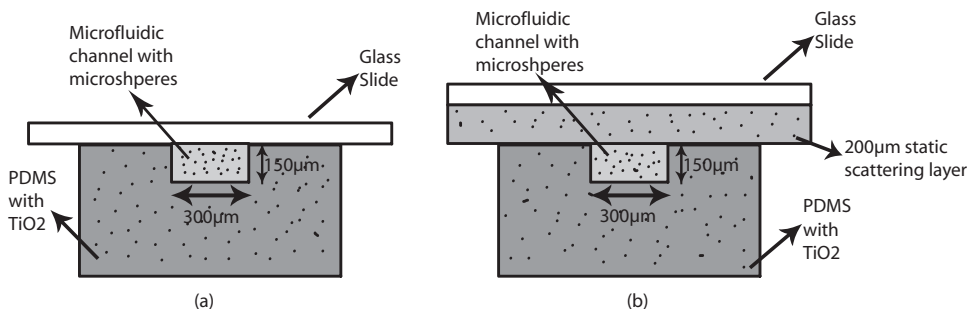

Fig. 2. Cross-section of microfluidic flow phantom (not to scale) (a) Without Static scattering layer, (b) With Static scattering layer. Samples were imaged from the top

We used a microfluidic device as a flow phantom. A microfluidic device as a flow phantom has the advantage of being realistic and cost effective, providing flexibility in design, large shelf life and robust operation. Our channels were rectangular in cross section (300 μm wide x 150 μm deep). The device was fabricated in poly dimethyl siloxane (PDMS) using the rapid prototyping technique [28]. Titanium dioxide (TiO_2) was added to the PDMS [29] (1.8 mg of TiO_2 per gram of PDMS) to give the sample a scattering background to mimic tissue optical properties. The prepared samples were bonded on a glass slide to seal the channels as shown in Fig. 2. The sample was connected to a mechanical syringe pump (World Precision Instruments, Saratosa, FL, USA) through silicone tubes, and a suspension ($\mu_s = 250$ cm^{-1}) of 1 μm diameter polystyrene beads (Duke Scientific Corp., Palo Alto, CA, USA) was pumped through the channels. For the static scattering experiments, a 200 μm layer of PDMS with different concentrations of TiO_2 (0.9 mg and 1.8 mg of TiO_2 per gram of PDMS corresponding to $\mu_s' = 4$ cm^{-1} and $\mu_s' = 8$ cm^{-1} respectively) was sandwiched between the channels and the glass slide, to simulate a superficial layer of static scattering such as a thinned skull (Fig. 2(b)). The reduced scattering coefficients of the 200 μm static scattering layer were estimated using an approximate collimated transmission measurement through a thin section of the sample. Fig. 2 shows a schematic of the cross-section of the devices.

4. Results

The experimental setup (Fig. 1) was used in conjunction with the exposure modulation technique to perform controlled experiments on the microfluidic samples. The microfluidic sample without the static scattering layer (Fig. 2(a)) was used to test the accuracy of the multi-exposure speckle imaging instrument (MESI) and the new speckle model. As detailed earlier (Section 3) the suspension of micro spheres was pumped through the sample using the syringe pump at different speeds from 0 mm/sec (Brownian motion) to 10 mm/sec in 1 mm/sec increments. 30 speckle contrast images were calculated and averaged for each exposure from the raw speckle images. The average speckle contrast in a region within the channel was calculated. We note that in this fully dynamic case, the static spatial variance v_s is very small. v_s would be dominated by the experimental noise v_{noise} as the ergodicity assumption would be valid and $v_{ne} \approx 0$. β is one of the unknown quantities in Eq. 11 describing speckle contrast. Theoretically, β is a constant that depends only on experimental conditions. An attempt to estimate β using a reflectance standard would yield inaccurate results due to the presence of the static spatial vari-
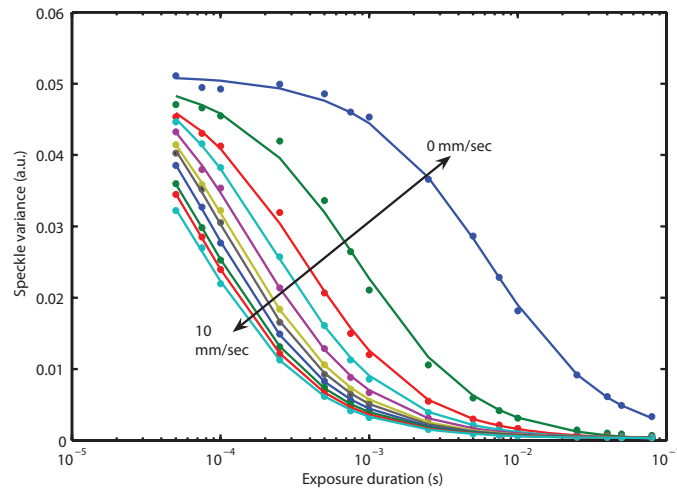
Fig. 3. Multi-Exposure Speckle Contrast data fit to new speckle model. Speckle variance as a function of exposure duration for different speeds. Measurements were made on samples with no static scattering layer (Fig. 2(a))

ance v_s. Here the ergodicity assumption would breakdown, and v_{ne} would be significant. We would be unable to separate the contributions of speckle contrast from β, v_{ne} and v_{noise}. Instead the value of β was estimated, by performing an initial fit of the multi-exposure data to Eq. 4 with the addition of v_s, while having β, τ_c and v_s as the fitting variables. The speckle contrast data was then fit to Eq. 11 using the estimated value of β and the results are shown in Fig. 3. Holding β constant ensures that the fitting procedure is physically appropriate and makes the search space of the nonlinear optimization process more reasonable and computationally less intensive. Fig. 3 clearly shows that the model fits the experimental data very well (mean sum squared error: 2.4×10^{-6}). The correlation time of speckles was estimated by having τ_c as a fitting parameter. The standard error of correlation time estimates was found using bootstrap re-sampling. Correlation times varied from 3.361 ± 0.17ms for Brownian motion to $38.4 \pm 1.44 \mu$s for 10mm/sec. The average percentage error in estimates of correlation times was 3.37%, with a minimum of 1.99% for 3mm/sec and a maximum of 5.2% for Brownian motion. Other fitting parameters were v_s, the static spatial variance and ρ, the fraction of dynamically scattered light. We note that *a priori* knowledge of ρ is not required for us to obtain τ_c estimates. Hence this technique can be applied to cases where the thickness of the skull is unknown and/or variable.

In order to verify our argument on nonergodicity, we compared the speckle contrast obtained using spatial analysis [1, 2] and temporal analysis [24, 25]. Spatial speckle contrast was estimated by using Eq. 1 and the procedure detailed earlier, while temporal speckle contrast was estimated by calculating the ratio of the standard deviation to mean of the intensities of a single pixel over different frames at the same exposure duration. We performed multi-exposure speckle contrast measurements on the microfluidic devices with different levels of static scattering in the static scattering upper layer (Fig. 2(a): $\mu_s' = 0$ cm^{-1} and Fig. 2(b): $\mu_s' = 4$ cm^{-1} and $\mu_s' = 8$ cm^{-1}). A suspension ($\mu_s = 250$ cm^{-1}) of 1 μm diameter polystyrene beads was pumped through the channels at 2 mm/sec. The experimentally obtained temporal contrast (temporal sampling) and spatial contrast (ensemble sampling) curves for each static scattering case is shown in Fig. 4.

From Fig. 4 we can clearly see that the temporal contrast curves (dotted lines) do not possess
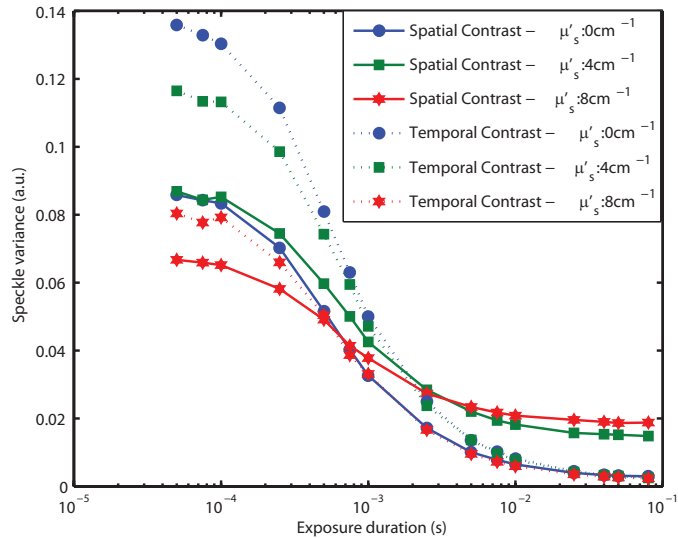
Fig. 4. Multi-Exposure Speckle Contrast data analyzed by spatial (ensemble) sampling (Solid lines) and temporal (time) sampling (dotted lines). Measurements were made at 2 mm/sec. The three curves for each analysis technique represent different amounts of static scattering. μ_s' values refer to the reduced scattering coefficient in the 200 μm static scattering layer. $\mu_s' = 0$ cm^{-1}: No static scattering layer (Fig. 2(a)), $\mu_s' = 4$ cm^{-1}: 0.9 mg/g of TiO$_2$ in static scattering layer (Fig. 2(b)), $\mu_s' = 8$ cm^{-1}: 1.8 mg/g of TiO$_2$ in static scattering layer (Fig. 2(b)). Speckle variance curves show that the nonergodic variance v_{ne} is absent in all three temporally sampled curves and in the completely dynamic spatially (ensemble) sampled curve. v_{ne} is significant in the cases with a static scattered layer, when the data is analyzed by spatial (ensemble) sampling.

a significant constant variance since the variance approaches zero at long exposure durations. The small offset that we observe is likely due to v_{noise} which remains constant even in the presence of static scattering and does not change as the amount of static scattering increases. However, the spatial (ensemble sampled) contrast curves (solid lines) show a clear offset at large exposure durations when static scatterers were present. We also notice that this offset increases with an increase in static scattering. Again, when no static scatterers were present, the spatial (ensemble sampled) contrast curve does not possess this offset. This provides evidence in favor of the argument that the increase in variance at large exposure durations is due to v_{ne}, the nonergodic variance. We also notice that for the same static scattering level, the variance obtained by temporal sampling is greater than the variance obtained by spatial sampling. This could be due to different β. Though both spatial and temporal speckle visibility increase as the speckle size approaches the size of a detector element of the camera, once the speckle size is greater than a detector element the speckle visibility should not change for the temporal case, while acquiring multiple samples from a single speckle in the spatial case will tend to decrease the speckle visibility. This could lead to the two processing techniques to posses different β values. We note that our objective here is not to compare temporal speckle contrast with spatial speckle contrast, but to utilize the two curves to provide evidence in favor of our model and hypothesis.

One of the significant improvements that the new speckle model provides is its ability to estimate correlation times consistently in the presence of static scatterers. We repeated the flow
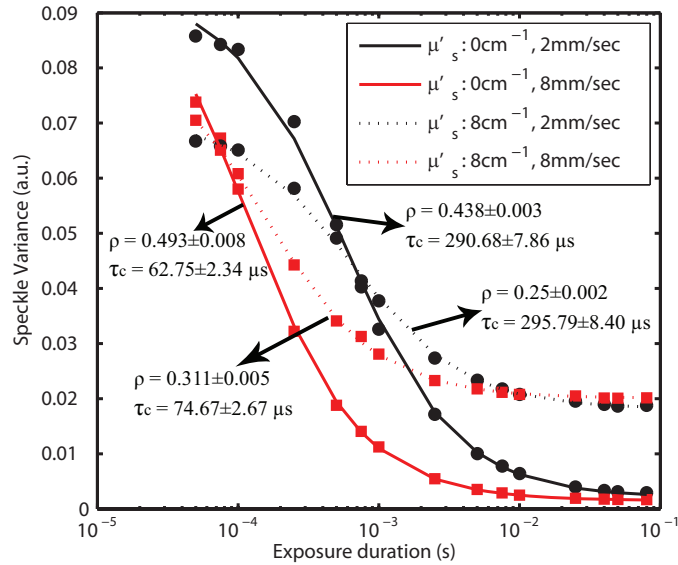
Fig. 5. Multi-Exposure Speckle Contrast data from two samples fit to the new speckle model. Speckle variance as a function of exposure duration for two different speeds and two levels of static scattering. Solid lines represent measurements made on sample without static scattering layer. Dotted lines represent measurements made on sample with static scattering layer. μ'_s values refer to the reduced scattering coefficient in the 200 μm static scattering layer. $\mu'_s = 0$ cm^{-1}: No static scattering layer (Fig. 2(a)), $\mu'_s = 8$ cm^{-1}: 1.8 mg/g of TiO$_2$ in static scattering layer (Fig. 2(b)).

measurements as detailed earlier, at speeds 0 mm/sec to 10 mm/sec in 2 mm/sec increments. Measurements on the sample with no static scattering layer (Fig. 2(a)) served as base (or 'true') estimates of correlation times. Fig. 5 shows the results of this analysis at two different speeds. Clearly, the addition of the static scattering layer drastically changes the shape of the curve. For a given speed, the decrease in variance at the low exposures is due to the relative weighting of the two exponential decays in Eq. 11 which is consistent with results obtained with DLS measurements [23]. The increase in variance at the larger exposure durations is due to the addition of the nonergodic variance v_{ne}. We also note that the new speckle model fits well to the data points. Also, the ρ values decrease with the addition of static scattering, implying a reduction in the fraction of total light that is dynamically scattered. It is important to note that for a given exposure duration and speed, the measured speckle contrast values are different in the presence of static scattered light when compared to the speckle contrast values obtained in the absence of static scattered light. Hence accurate τ_c estimates cannot be obtained with measurements from a single exposure duration without an accurate model and *a priori* knowledge of the constants ρ, β and v_s. These constants are typically difficult to estimate. By using the multi-exposure data and the updated model we are able to overcome this problem and reproduce τ_c consistently.

To quantify the effects of the static scattering layer on the consistency of the τ_c estimates we estimated the deviations in τ_c for each speed as the amount of static scatterer was varied. For each speed, the variation in the estimated correlation times over the three scattering cases (Fig. 2(a): $\mu'_s = 0$ cm^{-1}, Fig. 2(b): $\mu'_s = 4$ cm^{-1} and $\mu'_s = 8$ cm^{-1}) was determined by calculating the standard deviation of the correlation time estimates. This deviation was normalized to the base (or 'true') correlation time estimates. Single exposure estimates of correlation time
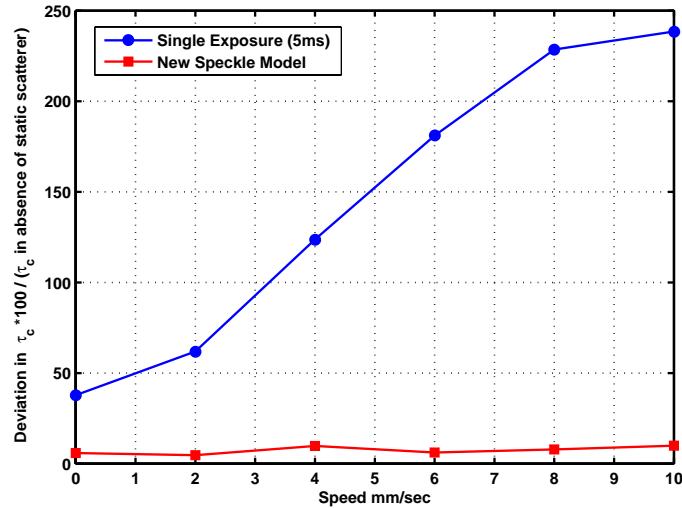
Fig. 6. Percentage deviation in τ_c over changes in amount of static scattering for different speeds (estimated using Eq. 12). Data from all three static scattering cases $\mu_s' = 0$ cm^{-1}: No static scattering layer (Fig. 2(a)), $\mu_s' = 4$ cm^{-1}: 0.9 mg/g of TiO$_2$ in static scattering layer (Fig. 2(b)), $\mu_s' = 8$ cm^{-1}: 1.8 mg/g of TiO$_2$ in static scattering layer (Fig. 2(b)) was used in this analysis. τ_c estimates with the new speckle model have extremely low deviation

were obtained using Eq. 3, which is appropriate because of its widespread use in most speckle imaging techniques to estimate relative flow changes. For an appropriate comparison, β was prefixed to Eq. 3, and same value of β was used for both the single exposure and MESI estimates. The results for the MESI model and the single exposure case are plotted in Fig. 6.

$$\% \text{ Deviation in } \tau_c = \frac{\text{Standard deviation in } \tau_c}{\tau_c \text{ in the absence of static scatterers}} \times 100 \tag{12}$$

Figure 6 clearly shows that the single exposure estimates are not suited for speckle contrast measurements in the presence of static scatterers. The error in the correlation time estimates is high and increases drastically with speed. The new speckle model performs very well, with deviation in correlation times being less than 10% for all speeds. This clearly shows that the new speckle model can estimate the correlation times consistently even in the presence of static scattering.

5. Discussion

One of the criticisms of LSCI has been the lack of quantitative accuracy of correlation time measures. This lack of quantitative accuracy can be attributed to several factors including inaccurate estimates of β and neglect of noise contributions and nonergodicity effects. The absence of the noise term in traditional speckle measurements can also lead to incorrect speckle contrast values for a given correlation time and exposure duration. The MESI instrument is aimed at reducing this experimental variability in measurements. Since images are obtained at different exposure durations the integrated autocorrelation function curve can be experimentally measured, and a speckle model can be fit to it to obtain unknown parameters, which include the characteristic decay time or correlation time τ_c, experimental noise and in the new speckle model, ρ, the fraction of dynamically scattered light. The MESI instrument also removes the

dependence of v_{noise} on exposure duration. The new speckle model and the τ_c estimation procedure allows for determination of noise with a constant variance. Without these improvements it would be very difficult to separate the variance due to speckle decorrelation and the lumped variance due to noise and nonergodicity effects.

We proceeded to test whether the τ_c estimates obtained using the MESI instrument were more accurate than traditional single exposure LSCI measures by comparing the respective estimates of the relative correlation time measures. Correlation time estimates from traditional single exposure measures was obtained using the procedure detailed earlier. Relative correlation time measures were defined as

$$\text{relative } \tau_c = \frac{\tau_{co}}{\tau_c}, \tag{13}$$

where τ_{co} is the correlation time at baseline speed and τ_c is the correlation time at a given speed. Correlation time estimates were obtained from the fits performed in Fig. 3, on multi-exposure speckle contrast data obtained with measurements made on the fully dynamic sample (Fig. 2(a)). The τ_c estimates obtained with the MESI instrument were compared with traditional single exposure estimates of τ_c at 1 ms and 5 ms exposures for their efficiency in predicting relative flows. Ideally, relative correlation measures would be linear with relative speed. Relative correlation times were obtained for a baseline flow of 2 mm/sec.

Figure 7 shows that the new speckle model used in conjunction with the multi-exposure speckle imaging instrument maintains linearity of relative correlation measures over a long range. Single exposure estimates of relative correlation measures are linear for small changes in flows, but the linearity breaks down for larger changes. The new multi-exposure speckle imaging instrument and the new speckle model address this underestimation of large changes in flow by traditional LSCI measurements. This comparison is significant, because relative correlation time measurements are widely used in many dynamic blood flow measurements. Traditional single exposure LSCI measures underestimate relative flows for large changes in
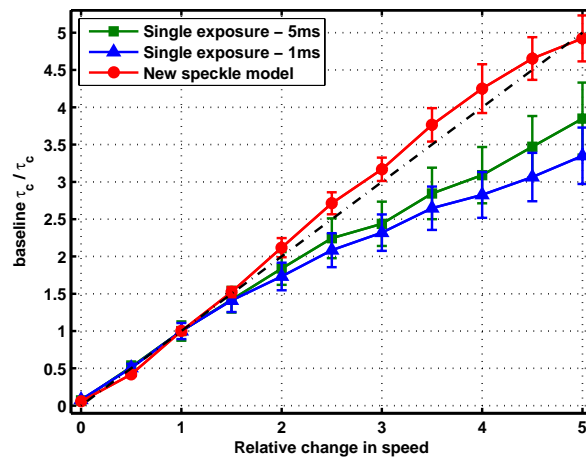

Fig. 7. Performance of different models to relative flow. Baseline speed : 2 mm/sec. Plot of relative τ_c to relative speed. Plot should ideally be a straight line (dashed line). Multi-Exposure estimates extend linear range of relative τ_c estimates. Error bars indicate standard error in relative correlation time estimates. Measurements made using microfluidic phantom with no static scattering layer (Fig. 2(a)).
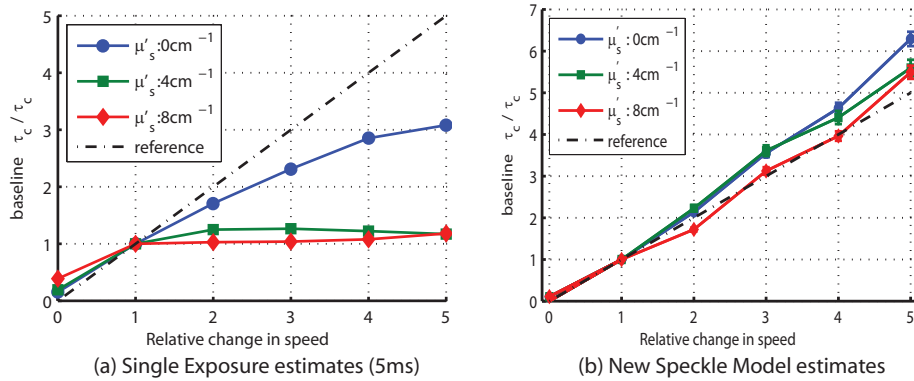
Fig. 8. Quantifying the effect of static scattering on relative τ_c measurements. Plot of relative correlation time (Eq. 13) to relative speed. Baseline Speed - 2 mm/sec. The three curves on each graph represent different amounts of static scattering. Error bars on (b) indicate standard error in estimates of relative correlation times. μ_s' values refer to the reduced scattering coefficient in the 200 μm static scattering layer. $\mu_s' = 0$ cm^{-1}: No static scattering layer (Fig. 2(a)), $\mu_s' = 4$ cm^{-1}: 0.9 mg/g of TiO$_2$ in static scattering layer (Fig. 2(b)), $\mu_s' = 8$ cm^{-1}: 1.8 mg/g of TiO$_2$ in static scattering layer (Fig. 2(b)). New speckle model retains the linearity of relative τ_c estimates.

flow. We have shown that the MESI instrument and the new speckle model can provide more accurate measures of relative flow.

Figure 7 also shows that even in a case where there is no obvious static scatterer like a thinned skull, there appears to be some contributions due to static scatterers, in this case possibly from the bottom of the channel in Fig. 2(a). While the fraction of static scatterers is not too significant, it appears to affect the linearity of the curve, and the MESI instrument with the new model can eliminate this error. We now investigate the effect of varying levels of static scattering on estimates of relative correlation times. We have shown earlier that the presence of the static scatterers significantly alters the shape of the integrated autocorrelation function curve in Fig. 5, for different speeds. We also showed that the new speckle model fits well to the experimentally determined speckle variance curve (Fig. 5) and that the new speckle model provides consistent estimates of τ_c even in the presence of static scatterers (Fig. 6). We proceeded to test whether the correlation time estimates obtained with the MESI instrument and the new speckle model maintained linearity for relative flow measurements (as in Fig. 7) in the presence of static scatterers.

Relative correlation time measures were obtained as detailed earlier (Eq. 13) using 2 mm/sec as the baseline measure. The new speckle model and traditional single exposure measurements (5 ms) were evaluated, and the results are shown in Fig. 8. Fig. 8 shows again why traditional single exposure methods are not suited for flow measurements when static scatterers are present. The linearity of relative correlation time measurements with single exposure measurements breaks down in the presence of static scatterers (Fig. 8(a)) while the new speckle model maintains the linearity of relative correlation time measures even in the presence of static scatterers (Fig. 8(b)). This again reinforces the fact that the MESI instrument with the new speckle model can predict consistent correlation times in the presence of static scatterers.

In our experiments we have tested our new instrument and new model for two different static scattering cases. Although the model yields robust estimates of τ_c in all cases that we tested,

the model will only work if the speckle signal from dynamically scattered photons is strong enough to be detected in the presence of the static background signal. Therefore, the model and the instrument will ultimately be limited by the signal to noise of the measurements. If the fraction of dynamically scattered photons is too small compared to statically scattered photons, the dynamic speckle signal would be insignificant and estimates of τ_c would breakdown. For practical applications, a simple single exposure LSCI image or visual inspection can qualitatively verify if there is sufficient speckle visibility due to dynamically scattered photons and subsequently the MESI instrument can be used with the new model to obtain consistent estimates of correlation times.

6. Conclusions

We presented a new speckle imaging instrument that has the capability to obtain speckle images over a wide range of exposure durations. We also presented a new speckle model that accounts for the presence of static scatterers. We show that the ergodicity assumption is violated in the presence of statically scattered photons and arrive at a potential solution to account for the presence of nonergodic light. We provide experimental evidence in support of our solution. We show that the Multi-Exposure Speckle Imaging (MESI) instrument when used in conjunction with the new speckle model extends the range over which relative correlation time measurements are linear. This addresses one of the major criticisms of speckle imaging that the linearity of relative correlation time measurements breaks down for large changes in speed. We also show that the new speckle model predicts correlation times consistently in the presence of static scatterers and that the new speckle model retains the linearity of relative correlation time measurements in the presence of varying concentration of static scatterers. Even though the relation between correlation time and average velocity is somewhat uncertain, quantitative estimation of the correlation time would enable calibrated flow measurements. Coupled with the ability to discriminate flows in the presence of static scatterers, the new multi-exposure speckle imaging instrument with the new speckle model would enable us to obtain a complete picture of cerebral blood flow.